The Astrophysical Journal, 654:487–493, 2007 January 1

THE ORIGIN AND MOTION OF PSR J0538+2817 IN S147

C.-Y. Ng,[1] Roger W. Romani,[1] Walter F. Brisken,[2] Shami Chatterjee,[2,3] and Michael Kramer[4]

Received 2006 August 26; accepted 2006 November 2

ABSTRACT

We report on Very Long Baseline Array (VLBA) astrometry and *Chandra* imaging of PSR J0538+2817 in the supernova remnant S147. We measure a parallax distance of $1.47^{+0.42}_{-0.27}$ kpc along with a high-precision proper motion, giving a transverse velocity $V_\perp = 400^{+114}_{-73}$ km s^{-1}. A small extended wind nebula is detected around the pulsar; the symmetry axis of this structure suggests that the spin axis lies $12^\circ \pm 4^\circ$ from the velocity vector (two-dimensional), but the emission is too faint for robust model-independent statements. The neutron star is hot, consistent with the young $\sim$40 kyr kinematic age. The pulsar progenitor is likely a runaway from a nearby cluster, with NGC 1960 (M36) a leading candidate.

Subject headings: astrometry — pulsars: individual (PSR J0538+2817) — stars: kinematics — supernovae: individual (S147)

1. INTRODUCTION

Sim 147 (S147, G180.0−1.7) is an optically faint shell-type supernova remnant (SNR) located in the direction of the Galactic anticenter. It is highly filamentary and has a radius of 83′ (Sofue et al. 1980). Although age estimates vary widely, from 20 kyr (Sofue et al. 1980) to 100 kyr (Kundu et al. 1980), S147 is believed to be one of the oldest SNRs with well-defined shell structure. It has been extensively studied at several wavelengths, including radio (Kundu et al. 1980; Sofue et al. 1980), optical (Lozinskaya 1976; Kirshner & Arnold 1979), UV (Phillips et al. 1981), and X-ray (Souvageot et al. 1990). A recent continuum-subtracted Hα image (Drew et al. 2005) reveals much detailed structure in S147. As shown in Figure 1, the shell is mostly circular with a few obvious blowouts to the east and the north. Gvaramadze (2006) suggested that a faint blowout to the west and the brighter lobe to the east define a bilateral axis passing through the center. Most of the bright filaments concentrate on the southern half, where the SNR boundary is also sharper. In contrast, the northern half is more diffuse and less well-defined.

Within the boundaries of S147, a 143 ms pulsar PSR J0538+2817 was discovered by Anderson et al. (1996) in an undirected pulsar survey using the 305 m Arecibo radio telescope. The pulsar has a large characteristic age $\tau_c = P/2\dot{P} = 620$ kyr and a dispersion measure (DM)–estimated distance of 1.2 kpc. On the basis of the positions and distances of PSR J0538+2817 and S147, Anderson et al. (1996) suggested an association between the two. From the maximum SNR age of 10^5 yr, Romani & Ng (2003) argued that PSR J0538+2817 had a slow initial spin period. This was supported by Kramer et al. (2003), who obtained a rough timing proper motion that indicated that the pulsar is moving from near the SNR geometrical center with a kinematic age of only 30 kyr, much shorter than the characteristic age. To reconcile the discrepancy, they also suggested a large initial spin period of 139 ms for the pulsar. Alternatively, Gvaramadze (2006) proposed that PSR J0538+2817 arose in the first supernova from a massive binary, while a second supernova produced S147. In X-rays, PSR J0538+2817 has been detected by *ROSAT* All Sky Survey (Sun et al. 1996) and High Resolution Imager imaging. A 20 ks *Chandra* ACIS-S observation discovered extended emission around the pulsar (Romani & Ng 2003), while an *XMM-Newton* observation (McGowan et al. 2003) reported the detection of pulsed X-ray emission.

In summary, S147, with an old nearly circular shell and a central pulsar showing extended X-ray emission, provides some unique opportunities to test the details of the pulsar/SNR connection. Kinematic measurements, along with X-ray morphology and cooling measurements, can probe the history of the pulsar.

2. PARALLAX AND PROPER MOTION MEASUREMENT

PSR J0538+2817 was observed with the NRAO VLBA over nine epochs between 2002 and 2006. The observations were conducted between 1.4 and 1.7 GHz, as a trade-off between increasing pulsar flux at lower frequencies and improved resolution as well as reduced ionospheric effects at higher frequencies. At each epoch, four spectral windows (intermediate frequencies [IFs]), each with 8 MHz bandwidth, are observed simultaneously. To retain visibility phase coherence, repeated visits were made to the primary phase calibrator source 133′ distant from the pulsar. A VLA survey of the region around J0538+2817 revealed a compact 8 mJy source only 8′ distance from the pulsar; the two sources are within the same VLBA primary beam and were observed simultaneously. The data were correlated in two passes, first centered on the pulsar field, and then a second pass centered on the in-beam calibrator. The signal-to-noise ratio for the pulsar was boosted by "gating" (accepting signal from) the correlator on at the expected times of arrival of pulses, using current pulse timing solutions obtained for each epoch from ongoing observations at the Jodrell Bank Observatory. Incremental phase calibration derived from observations of the in-beam source were applied to the pulsar for considerably improved calibration.

Data analysis was performed using the AIPS package with a customized pipeline (W. F. Brisken 2007, in preparation), which included amplitude calibration based on the system temperatures and antenna gains, followed by visibility phase calibration based on the primary calibrator and the in-beam source. Large-scale ionospheric phase effects were estimated and corrected with the AIPS task `tecor`, using global models of the ionospheric electron content based on distributed GPS measurements. Once the

[1] Department of Physics, Stanford University, Stanford, CA 94305; ncy@astro.stanford.edu, rwr@astro.stanford.edu.
[2] National Radio Astronomy Observatory, P.O. Box O, Socorro, NM 87801; wbrisken@aoc.nrao.edu.
[3] Harvard-Smithsonian Center for Astrophysics, 60 Garden Street, MS 67, Cambridge, MA 02138; schatterjee@cfa.harvard.edu.
[4] Jodrell Bank Observatory, University of Manchester, Macclesfield, Cheshire SK11 9DL, UK; mkramer@jb.man.ac.uk.

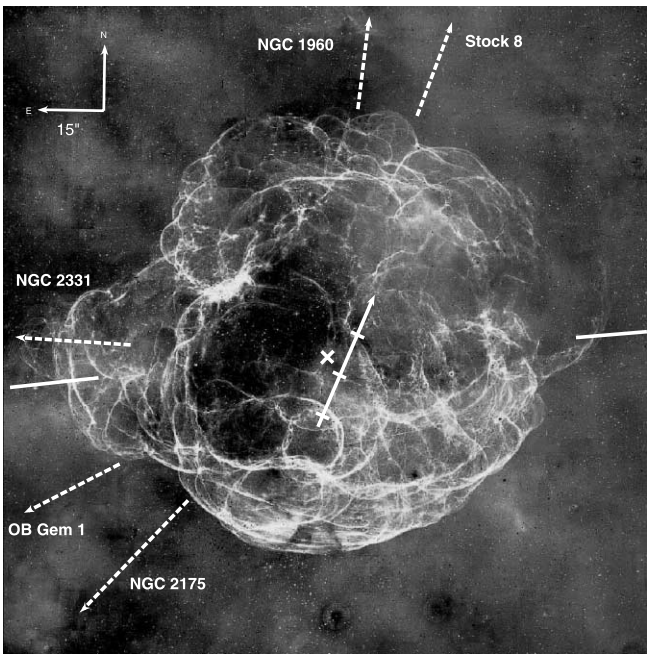

FIG. 1.—Continuum-subtracted Hα image of S147 (Drew et al. 2005). The arrow in the center shows the pulsar's proper motion direction and points to its current position (see § 2), with tick marks indicating the birth sites of the pulsar if born 20, 40, and 60 kyr ago. The cross marks the SNR geometrical center suggested by Kramer et al. (2003). Solid lines mark a possible bilateral axis (Gvaramadze 2006), and dashed lines show the direction to several candidate birth sites for the progenitor star.

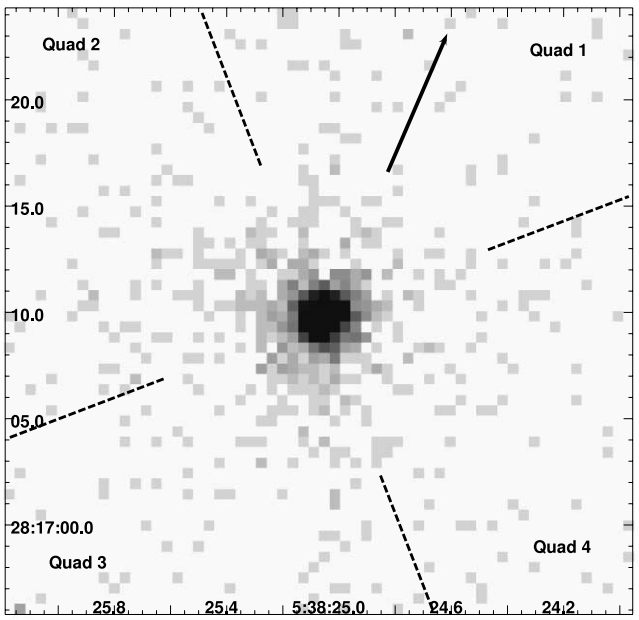

FIG. 2.—ACIS-I 0.5–8 keV image. The arrow indicates the pulsar's proper motion direction in its LSR. The dashed lines separate the four quadrants used to measure the azimuthal distribution of the extended emission.

calibration was completed, the pulsar position was measured by fitting a Gaussian ellipse to calibrated images made separately for each IF. The pulsar parallax and proper motion were then obtained from a linear least-squares fit to the epoch positions.

Table 1 shows the best-fit astrometric results from eight good epochs, for which the pulsar is far away from the Sun, with IFs equally weighted. The derived pulsar distance and transverse velocity are $d = 1.47^{+0.42}_{-0.27}$ kpc and $V_\perp = 400^{+114}_{-73}$ km s^{-1}, respectively. The distance is in good agreement with the DM-estimated value $d_{\rm DM} = 1.2 \pm 0.2$ kpc, using the NE2001 model (Cordes & Lazio 2002). The proper motion is also consistent with the timing observation results reported by Kramer et al. (2003), but our errors are much smaller, especially in the ecliptic latitude (μ_β). To convert the proper motion to its local standard of rest (LSR), we correct for differential Galactic rotation using $\Omega_0 = 220$ km s^{-1}, $R_0 = 8.5$ kpc (Fich et al. 1989) and the solar constants 10 ± 0.36, 5.25 ± 0.62, 7.17 ± 0.38 km s^{-1} (Dehnen & Binney 1998). The corrected proper motion is $\mu_* = 58.51 \pm 0.18$ mas yr^{-1} at position angle (P.A.) $336\overset{\circ}{.}8 \pm 0\overset{\circ}{.}13$, which converts to a transverse velocity of $V_\perp = 407^{+116}_{-74}$ km s^{-1}. Backward extrapolation of the pulsar's motion indicates that it passed $\sim 8'$ from the geometrical center of S147 defined by Kramer et al. (2003) at $\alpha = 05^{\rm h}40^{\rm m}01^{\rm s} \pm 2^{\rm s}$, $\delta = 27^\circ 48' 09'' \pm 20''$ (J2000.0). Since the pulsar is young and located near the Galactic plane, this trajectory is not significantly altered by acceleration in the Galactic potential. For any reasonable Galactic model (e.g., in Sun & Han [2004] and references therein), the displacement from a linear trajectory over the pulsar characteristic age is much smaller than $1'$. However, the SNR and pulsar are almost certainly associated (see below), and thus we conclude that the nominal center of the shell does not represent the explosion site and that S147 underwent asymmetric expansion, likely due to inhomogeneities in the surrounding interstellar medium.

TABLE 1
PARAMETERS FOR PSR J0538+2817

Parameter	Value
Epoch (MJD)	53,258
R.A. (J2000.0)	$05^{\rm h}38^{\rm m}25\overset{\rm s}{.}05237 \pm 0\overset{\rm s}{.}00001$
Decl. (J2000.0)	$+28^\circ 17' 09\overset{''}{.}3030 \pm 0\overset{''}{.}0001$
$\mu_{\alpha \cos\delta}$ (mas yr^{-1})	-23.53 ± 0.16
μ_δ (mas yr^{-1})	52.59 ± 0.13
π (mas)	0.68 ± 0.15
d (kpc)	$1.47^{+0.42}_{-0.27}$
$V_\perp$ (km s^{-1})	400^{+114}_{-73}
l, b (deg)	179.7186, -1.6859
μ_l, μ_b (mas yr^{-1})	-57.03, 8.18
n_e (cm^{-3})	0.027 ± 0.006

3. *CHANDRA* OBSERVATIONS

Chandra observations of PSR J0538+2817 were carried out on 2006 January 18 and 20 (Observation IDs 6242 and 5538) with the ACIS-I array operating in very faint timed exposure (VFTE) imaging mode. The pulsar was positioned near the aim point on the I3 chip, which was the only chip active during the observation. Subarray mode with 160 rows was used to further reduce the CCD pile-up. The resulting frame time of 0.5 s reduced the pile-up of the pulsar to 2%, ensuring the distortion of the point-spread function (PSF) and the high-energy spectrum is minimal. The total live time was 93.2 ks and examination of the background light curve showed no strong flares during the observation. Hence, all data are included in the analysis.

For comparison, we have also reprocessed the archival 20 ks ACIS-S exposure (ObsID 2796 [obs/02796]) observed on 2002 February 7. After filtering out the periods suffering from background flares, 18.5 ks of clean exposure remains. All data analysis was performed using CIAO 3.3 and CALDB 3.2.1 to ensure the latest time-dependent gain calibration and charge transfer inefficiency (CTI) correction are applied. To further improve the spatial

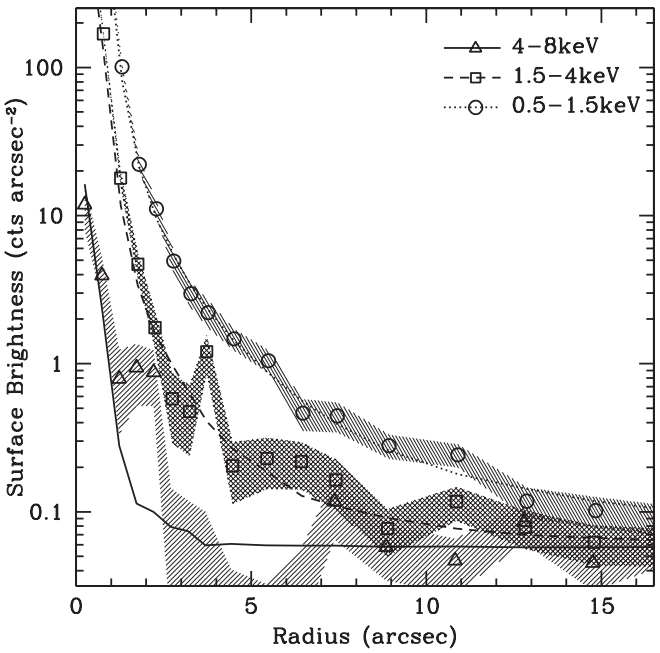

FIG. 3.—Observed source (*symbols*) and model point source (*lines*) radial count distributions in three energy bands, with the corresponding uncertainties (*shaded bands*).

resolution, we removed the ACIS pixel randomization and applied the algorithm by Mori et al. (2001) to correct the position of split pixel events.

4. SPATIAL ANALYSIS

The ACIS-I 0.5–8 keV image is shown in Figure 2. The point source produces 0.12 counts s^{-1}. With the short frame time, a trail of counts can be seen along the readout direction (at P.A. 5°), with 0.5 counts $pixel^{-1}$. The extended emission $\sim 5''$ northeast of the pulsar reported by Romani & Ng (2003) is clearly detected in the new observation. However, the deeper exposure shows that the structure is not an obvious torus. It also appears somewhat fainter in the new data, with $(4.3 \pm 0.7) \times 10^{-4}$ counts s^{-1} in 0.5–8 keV after background subtraction, as compared to $(9.7 \pm 2.2) \times 10^{-4}$ counts s^{-1} in the archival ACIS-S data. Diffuse emission is also seen in the southeast direction, as noted by Romani & Ng (2003) at $\sim 3''$ from the point source. Given that the direction is behind the pulsar's proper motion, this could be trailed emission from relativistic electrons in the motion-confined pulsar wind, as observed in other pulsar wind nebula (PWN) systems.

Figure 3 compares the observed surface brightness of the source for the ACIS-I data and the model PSF+background in three energy bands. The PSF is simulated using the Chandra Ray-Tracer (ChaRT) and MARX software using the best-fit pulsar spectrum from a $1''$ radius aperture, in order to minimize any nebular contamination. Although the readout trail is simulated in the model PSF, we excluded two rectangular regions of $1.5''$ wide along the readout trail and beyond $2.5''$ from the point source in our analysis, in order to improve the statistics. The graph suggests that the data and PSF model are well matched for the low-energy band, while excess counts appear at several radii for the higher energies.

To investigate the azimuthal distribution of these counts, we show in Figure 4 the PSFs and observed counts per unit area for the four quadrants (in three energy bands) with quadrant 1 along the proper motion direction (see Fig. 2). The shaded region shows the Poisson uncertainty in the surface brightness measurements. Here we see significant departures from the PSF in all three energy bands. The excesses from $4''$ to $6''$ and $9''$ to $11''$ in quadrant 2 in the low-energy band represents the candidate "torus" suggested in Romani & Ng (2003); no corresponding excess is seen in quadrant 4. A persistent excess is also seen from $4''$ to $8''$ in quadrant 3 of the medium energy band, representing the diffuse emission trailing behind the pulsar.

Most intriguing, however, is the very significant excess seen in the 4–8 keV band from $2''$ to $4''$ (Fig. 3). In Figure 4 we see that this lies in quadrants 2 and 4, indicating significant structure with a hard spectrum very close to the pulsar. The 4–8 keV ACIS-I image (Fig. 5) in fact shows a clear symmetric, almost linear structure extending $\sim 2.5''$ from the pulsar. Realizations of the 4–8 keV model PSF are nearly circular and show no obvious spikes. With only 32 counts, we cannot resolve any details or assign a clear origin for this emission; however, it should be noted that the X-ray images of many other young neutron stars show polar jets or equatorial tori. *If* this is the case for PSR J0538+2817, the symmetry axis could indicate the pulsar spin axis. More

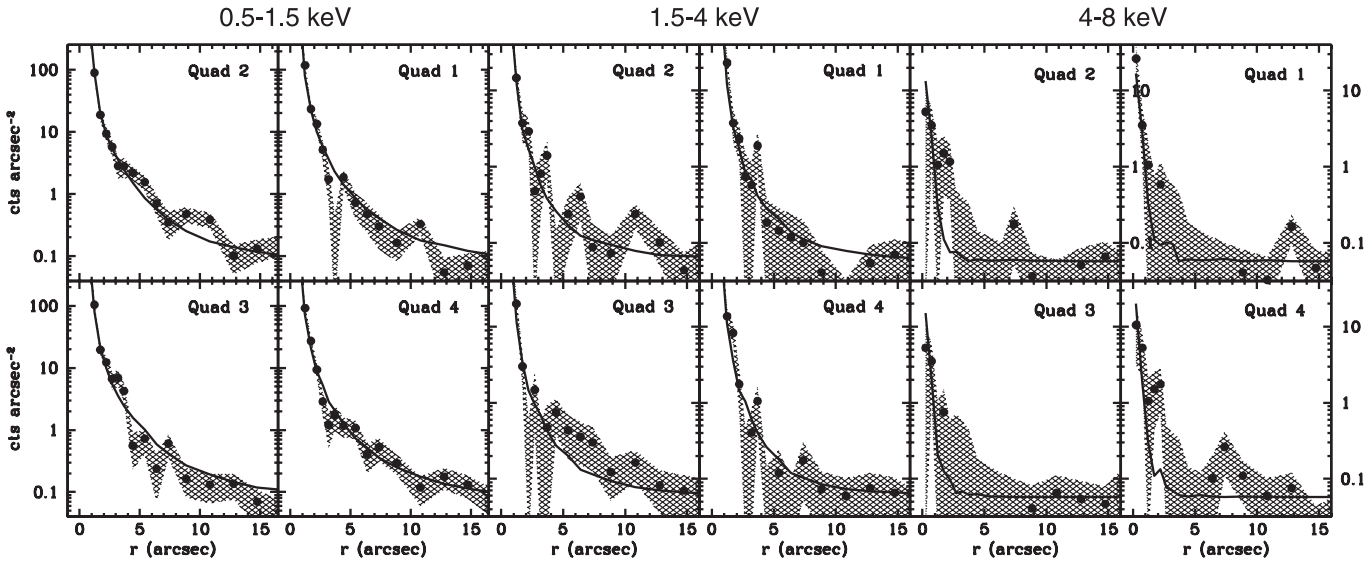

FIG. 4.—Surface brightness of the observed source (*filled circles*) and model point source (*lines*) for the four quadrants in three energy bands. The *y*-scale on the left applies to the 0.5–1.5 keV panel only, while the right scale applies to the other two panels.

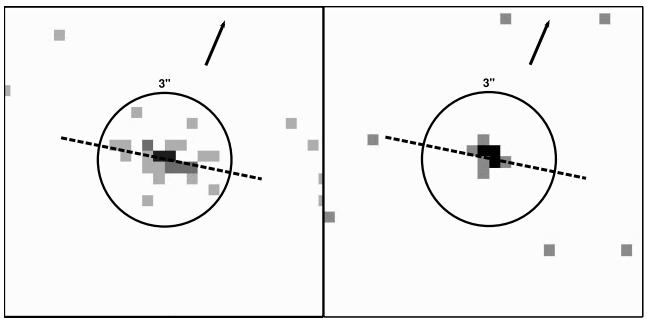

FIG. 5.—*Left*: ACIS-I 4–8 keV image with the dashed line showing the best-fit P.A. of the counts. The arrow indicates the pulsar's proper motion in its LSR. The circle is 3″ in radius. *Right*: Model PSF in the same energy band.

importantly, its alignment with the proper motion could constrain the pulsar kick physics (Romani 2005; C.-Y. Ng & R. W. Romani 2007, in preparation). In order to measure the P.A. of the symmetry axis quantitatively, the photon positions were fitted to a straight line passing through the point source. Linear least-squares fitting was employed and we obtained the best-fit P.A. at $79^\circ \pm 4^\circ$.

Although the 4–8 keV excess is statistically significant, interpretation of such faint compact structure is of course very uncertain. Some information on the pulsar orientation may be gleaned from the radio polarization measurements of Kramer et al. (2003), which suggest a magnetic inclination $\alpha = 95^\circ$ and impact angle $\sigma = 2^\circ$, implying a spin axis inclination of $\zeta = \alpha + \sigma \approx 97^\circ$, i.e., very nearly in the plane of the sky. This means that both the polar jet interpretation (with the near-orthogonal view implying similar jet/counterjet fluxes) and the equatorial torus interpretation (with a thin nearly edge-on torus) remain viable. If the extended emission is interpreted as polar jets, then the pulsar spin axis is 78° off the proper motion direction. This is much larger than any of the other pulsar/PWN systems. If the axis is the equatorial (torus) plane, then the inferred spin vector is at P.A. 169° (-11°), i.e., 12° off the velocity vector.

A statistical argument in fact supports the latter interpretation. If the spin axis and proper motion axis are orthogonal in true space, then most observed orientations make the projected angle on the plane of the sky smaller. If they are aligned, the projected angle tends to remain nearly aligned. For completely random orientations, 90% of vectors separated by 0°–10° retain a two-dimensional angle $\leq 10^\circ$; for vectors separated by 80°–90°, only 29% retain $\theta_{2D} \geq 80^\circ$. Thus, the observed angle is, a priori, $\sim$3 times more likely to arise from an aligned system. One additional piece of evidence could be extracted from absolute position angle measurements of the radio polarization (e.g., Johnston et al. 2005). Although mode ambiguity allows a 90° jump in the inferred projected field, these authors note that most pulsars appear to emit in the orthogonal mode, which may allow one to discriminate between the jet and torus interpretation.

5. SPECTRAL ANALYSIS

We now turn to the spectral analysis of the point source. For the best possible constraints on the spectrum, we have reprocessed both the 18.5 ks cleaned ACIS-S data set and our new 93 ks ACIS-I data with the latest time-dependent gain calibration and charge transfer inefficiency (CTI) correction. The source spectrum was extracted from a 2″ radius aperture with the script `psextract`, and the response matrix files (RMFs) were replaced by the ones built using the tool `mkacisrmf`, which accounts for the CTI. To model the aperture corrections, 10 PSFs with monochromatic energies from 0.5 to 9.5 keV were simulated using ChaRT. The fractional energy encircled by the aperture as a function of energy is obtained, and then used to correct the ancillary response files (ARFs). As the ACIS-S data suffer 20% pile-up, the CCD pile-up model by Davis (2001) is used in all the spectral fits.

Results from the combined fits of the ACIS-S and ACIS-I data sets are listed in Table 2. All fits are to the 0.3–8 keV range and the spectral parameter errors reported are projected multidimensional 1 σ values. For the uncertainties in flux (and hence stellar radius), as is often the case with low-statistic CCD-quality data, the projected errors are very large due to uncertainties in spectral parameters. Therefore we followed other authors in reporting the single parameter (i.e., one-dimensional) 1 σ error for the flux.

The source spectrum is adequately fitted by an absorbed blackbody. The best-fit $N_{\rm H} = 2.47 \times 10^{21}$ cm^{-2} is lower than the previous *Chandra* results, but consistent with the *XMM-Newton* measurements. Comparison with the DM value of 39.7 pc cm^{-3} gives $n_{\rm H}/n_e = 24$, which is relatively large. At the pulsar distance of 1.47 kpc, the best-fit spectral parameters give an effective blackbody radius of $R_\infty^{\rm eff} = 2.19$ km. This is too small to be reconciled with the whole stellar surface, but the flux could be hot $T \sim 2 \times 10^6$ K emission from a small fraction of the stellar surface ($\sim$2.7% for an $R_\infty = 13.1$ km star), possibly due to some heating mechanism such as bombardment of the polar cap regions by relativistic particles from the magnetosphere. The thermal radiation from the neutron star surface could also be described by atmospheric models. Light-element neutron star atmosphere models, such as those dominated by hydrogen, have large Wien excesses. This gives a lower effective temperature and hence larger stellar radius in the fit. We use here a pure H model with $B = 10^{12}$ G (Pavlov et al. 1991; Zavlin et al. 1996), as the inferred surface magnetic field strength of PSR J0538+2817 is 7×10^{11} G (Anderson et al. 1996). During the fit, the mass of the neutron star is held fixed at $M = 1.4\ M_\odot$ and the normalization constant is fixed using the pulsar distance. The best-fit surface temperature and radius are $T_\infty^{\rm eff} = 1.05 \times 10^6$ K and $R_\infty = 11.2$ km. As expected, this model suggests a lower effective temperature covering a

TABLE 2
SPECTRAL FITS TO PSR J0538+2817

		Blackbody/Atmosphere				Power Law ($\Gamma = 1.5$)		
Model	$N_{\rm H}$ (10^{21} cm^{-2})	T_∞ (10^6 K)	R_∞ (km)	Absorbed Flux $f_{0.5-8}$ (10^{-13} ergs cm^{-2} s^{-1})	Unabsorbed Flux $f_{0.5-8}$ (10^{-13} ergs cm^{-2} s^{-1})	Absorbed Flux $f_{0.5-8}$ (10^{-13} ergs cm^{-2} s^{-1})	Unabsorbed Flux $f_{0.5-8}$ (10^{-13} ergs cm^{-2} s^{-1})	χ^2/dof
BB	$2.47^{+0.15}_{-0.14}$	$2.11^{+0.03}_{-0.04}$	2.19 ± 0.01	7.24 ± 0.07	17.4 ± 0.2	...	...	109.7/139
Atm	$2.94^{+0.07}_{-0.06}$	1.05 ± 0.05	11.16 ± 0.02	7.21 ± 0.08	21.4 ± 0.2	...	...	120.7/139
BB+PL	2.50 ± 0.15	$2.10^{+0.04}_{-0.03}$	2.23 ± 0.01	7.15 ± 0.07	17.5 ± 0.2	0.20 ± 0.06	0.24 ± 0.07	99.5/138
Atm+PL.....	2.95 ± 0.07	$1.06^{+0.06}_{-0.05}$	10.99 ± 0.02	7.14 ± 0.08	21.4 ± 0.2	0.20 ± 0.05	0.24 ± 0.07	110.2/138

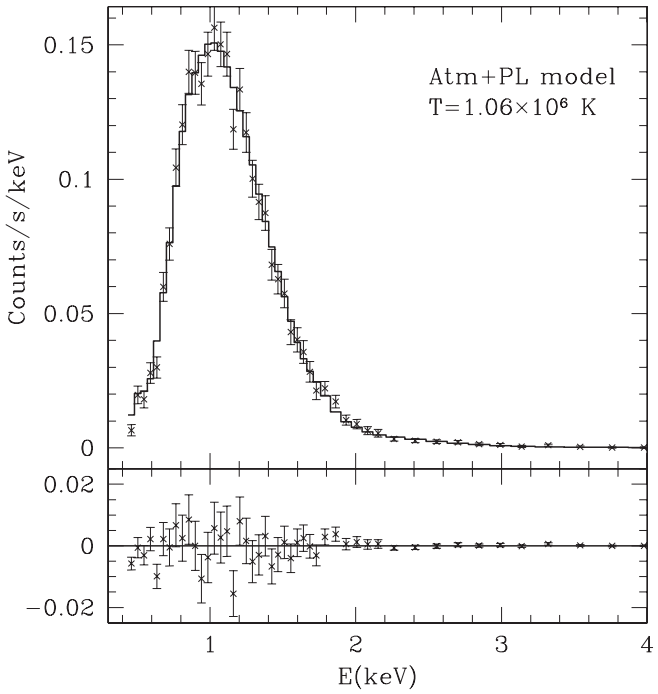

FIG. 6.—Point-source spectrum with a pileup-corrected magnetic H model atmosphere+power-law spectrum and residuals.

large fraction of the neutron star surface for a canonical radius. The fit is statistically slightly worse than that of the blackbody model, but both produce quite acceptable χ^2 values.

The extended emission observed at high energies suggests some flux in the 2″ aperture is contributed by nonthermal emission. Therefore we tried adding a power law component with fixed $\Gamma = 1.5$ to the models. Although the results are not improved substantially, the nonthermal flux is detected at >3 σ level as shown in the table; the effect on the parameters fitted for the thermal component is very small. The best-fit atmosphere+power-law model is shown in Figure 6.

6. DISCUSSION

6.1. *PSR J0538+2817/S147 Association*

The association between PSR J0538+2817 and S147 suggested by Anderson et al. (1996) was based on their positional coincidence and apparent consistency of the distances and ages. In particular, the authors argued that since the pulsar location is near the SNR center, it is unlikely to be a chance association. With our accurate proper motion measurement we can improve this argument. In order to have a quantitative estimate of the chance alignment probability, we did simple Monte Carlo simulations using the model by Faucher-Giguère & Kaspi (2006). Following these authors, we assume the pulsars are born in the Galactic plane with the galactocentric radial distribution from Yusifov & Küçük (2004) and exponential distribution in the scale height, and with birth velocities distributed as a two-component Gaussian model. Acceleration due to Galactic potential was ignored for simplicity. Our results show that in 2×10^5 yr, the most extreme age estimate for S147, only 1 pulsar in 2×10^7 would have a chance passage within 8′ of the S147 center. We also applied the Maxwellian pulsar velocity distribution suggested by Hobbs et al. (2005) obtaining nearly identical result. With a Galactic neutron star birthrate of 2.8 per century (Faucher-Giguère & Kaspi 2006) and a radio beaming factor of ~1/5, the probability of finding a random, unassociated radio pulsar younger than 1 Myr that has passed within 8′ of the SNR center is $\sim 3 \times 10^{-4}$. This estimate is a conservative upper limit to the probability: we believe the true age of S147 is considerably younger, and the high X-ray temperature of PSR J0538+2817 also implies a younger age, $\leq 10^5$ yr. Thus, a more realistic chance probability is $\geq$10 times smaller. To conclude, PSR J0538+2817 is almost certainly associated with S147, and this implies a SNR distance of ~1.5 kpc. This value is substantially larger than some previous estimates (e.g., Kundu et al. 1980), thus it calls into question some papers that assume a much closer distance to S147 (e.g., Phillips et al. 1981; Sallmen & Welsh 2004).

6.2. *S147 as a Cavity Explosion*

In standard SNR evolution, the shell radius in the Sedov-Taylor phase is given by $R_{\rm SNR} = 0.31(E_{51}/n_0)^{1/5} t^{2/5}$ pc (e.g., van der Swaluw 2001), where the explosion energy is $E_0 = 10^{51} E_{51}$ ergs, age in t years, and external medium of density n_0 cm^{-3}. The observed angular size of S147 $\theta = 83'$ (Sofue et al. 1980) corresponds to a physical radius of 35 pc at 1.47 kpc. For an age of 30 kyr (Kramer et al. 2003), this requires a very energetic explosion of $E_{51} = 20 n_0$. This suggests S147 probably occurred in a low-density stellar wind bubble, likely evacuated by the progenitor star in a Wolf-Rayet phase (Kramer et al. 2003; Gvaramadze 2006). Hence the SNR had a long free-expansion phase, only passing to the Sedov-Taylor phase when it reached the cavity boundaries at relatively large radius. This scenario receives further support from the observed low expansion velocity of S147 at 80 km s^{-1} (Kirshner & Arnold 1979). Note that the progenitor's proper motion can make the wind bubble asymmetric, with the cavity extending further behind the star (Gvaramadze 2006). Density gradients in the external medium can also enhance this asymmetry. Indeed gas and dust surveys suggest that the medium to the south of S147 is denser and the shell is flattened with the brightest filaments on this side. Supporting this, the optical observations by Lozinskaya (1976) provides some hint that the expansion rate is faster in the northern half of S147. Thus, we generally expect the geometrical center to lie somewhat north of the true explosion site.

6.3. *Birth Site of the Progenitor*

With the inferred distance to S147, it is possible to search for the birth site of its parent star. O and B stars are the direct progenitors of neutron stars, and the minimum mass for supernova explosion is $\sim 8 M_\odot$. These massive stars are generally formed in OB associations and young open clusters. With their short <50 Myr lifetimes they do not travel far from the birth sites. Typical peculiar velocities are a few km s^{-1}; for 10 km s^{-1}, we expect the progenitor to travel $\leq$500 pc. We compiled a list of open clusters and OB associations from the catalogs including Ruprecht et al. (1983), Mel'nik & Efremov (1995), Dias et al. (2002), and Kharchenko et al. (2005) and found only four candidates younger than 50 Myr with a nominal distance to S147 of <500 pc (Table 3). Directions to potential birth sites are shown in Figure 1.

With a three-dimensional spatial separation of only 220 pc from S147, NGC 1960 (M36) is the closest candidate. This is a relatively massive ~40 Myr old cluster (Kharchenko et al. 2005), and we consider it the prime candidate birth site. If correct, the progenitor traveled from this cluster at P.A. $\sim 175^\circ$ with a three-dimensional space velocity of $\sim 5(M/10\ M_\odot)^{2.5}$ km s^{-1}. We see no evidence in gas maps or the SNR shell that the progenitor wind has disturbed the denser cloud to the south. This and the blowouts of the SNR to the north argue against Gem OB 1 or NGC 2175 as

TABLE 3
Open Clusters Younger than 50 Myr within 500 pc of S147

Name	d (kpc)	θ (deg)	r (pc)	N^*	Age (Myr)
NGC 1960 (M36)	1.32	6.4	217	60	42
OB Gem 1	1.34	9.9	276	...	<5
NGC 2175	1.63	10.0	311	60	9
Cl Stock 8	1.82	7.1	405	40	41
NGC 2331	1.33	19.3	488	30	?

the parent cluster. Cl Stock 8 to the north remains viable, but is distant at $\geq$400 pc and less massive. Finally, it is intriguing to note that the fifth nearest young cluster, the very poorly studied NGC 2331, lies precisely in the direction of the largest (eastern) extension of the SNR shell; the Hα shell here extends 40% ($\sim$35′) further than the main shock front, with wispy emission present up to 10′ further in this direction. It is tempting to associate this blowout with a stellar wind trail extending along the path to NGC 2331, but this cluster appears to be relatively low mass and may be too old, with no remaining B stars.

6.4. *Explosion Site*

From the precise pulsar proper motion, we know that the supernova explosion must have occurred along the line in Figure 1 with the arrowhead at the present pulsar position. The explosion site is determined by the true age of S147/PSR J0538+2817; tick marks on the line indicate 20, 40, and 60 kyr ages. The simplest interpretation is to infer birth at the closest approach to the geometrical center 36 kyr ago and assign an uncertainty of $\sim 8'/57.6$ mas yr$^{-1} = 8$ kyr. However, if we can define a second axis for the progenitor motion, we can obtain a more precise age. If we adopt the symmetry axis suggested by Figure 1 (*solid lines*) of Gvaramadze (2006), then the birth site is to the northwest of the geometrical center and the intersection with the proper motion suggests a SNR age near 20 kyr. Given the rather irregular nature of the northern half of the remnant and the argument that the explosion should be south of the geometrical center, we do not find this axis convincing. The axis to NGC 2331 intersects at a more plausible explosion age of 30 kyr.

If, however, we adopt NGC 1960 as the birth site, then an explosion somewhat south of (in front of) the geometrical center becomes natural. Without a blowout identifying an entry site, we cannot set a precise axis, but the path should pass close to the geometric center, implying an intersection with the proper motion vector at $\leq$60 kyr. Our conclusion is that the best estimate of the SNR age is 40 kyr with a maximum plausible range of 20–60 kyr. This is slightly older than the estimate of Kramer et al. (2003). However, the inferred initial spin period of PSR J0538+2817 is not significantly changed. Assuming magnetic spin-down with constant braking index $n = 3$, the initial spin period is given by

$$P_0 = P\left(1 - \frac{n-1}{2}\frac{\tau}{\tau_c}\right)^{1/(n-1)},$$

where τ and τ_c are the kinematic and characteristic ages of the pulsar respectively. We obtained $P_0 = 138 \pm 2.3$ ms; the kinematic age of the pulsar is indeed much smaller than its spin-down age.

6.5. *Spin-Velocity Alignment*

Only a few pulsars have estimated initial spin periods; the value for PSR J0538+2817 is the longest among these. Of course, the high space velocity of the pulsar argues for a strong birth kick. Note that with the large parallax distance to the pulsar, the binary break-up scenario described by (Gvaramadze 2006) is now even more improbable. If one further accepts a progenitor origin in the Galactic plane near NGC 1960, then the pulsar's present rapid return to the plane further supports a birth kick uncorrelated with its parent's motion.

These considerations make a comparison of this pulsar's kick and spin direction particularly appealing. Unfortunately the morphology of the extended structure near the pulsar is not clear enough to define a definitive spin axis and thus weakens this system's ability to cleanly test the spin-kick models. However, we can turn the question around: if the mechanism that seems to cause spin and kick alignment in other young pulsars acts on PSR J0538+2817, do we expect its spin to be more nearly aligned or orthogonal? To retain a slow spin with a large kick velocity, the net kick vector must be nearly radial, applying little torque to the star.

We have performed a series of simulations of neutron star birth kicks in a range of models where a single thrust is applied to the surface at fixed angle as the proto–neutron star cools, with amplitude proportional to the driving neutrino luminosity (C.-Y. Ng & R. W. Romani 2007, in preparation). Comparing with the set of all neutron stars with initial spin and/or velocity measurements, we have found (for several models of proto–neutron star evolution and neutrino cooling) the best-fit parameter distributions for the neutron star prekick spin, kick amplitude, normal direction, and duration that reproduce the observed pulsar spin and speed distributions. For these parameters (fixed by a set of $\sim$50 other pulsars) we can ask whether a pulsar with slow initial spin like PSR J0538+2817 is more likely to have its birth velocity and spin vectors aligned or orthogonal. The simulations find that for $P \sim$ 140 ms, the aligned case is produced 30–90 times more frequently than the orthogonal cases, even though faster spin pulsars do not always show good alignment. C.-Y. Ng & R. W. Romani (2007, in preparation) discuss the significance of this result for improving kick constraints.

6.6. *Pulsar Thermal Emission*

From the X-ray spectral results, the neutron star atmosphere fit gives an effective surface temperature of $\gtrsim 10^6$ K. This matches well to the standard cooling curve for the pulsar age of $\lesssim$40 kyr (e.g., Fig. 6 in McGowan et al. 2003). Comparing with the cooling models of Yakovlev & Pethick (2004), we see that our best-fit 1.05×10^6 K surface agrees well with a typical cooling model at age 25 kyr. Even so-called slow cooling neutron stars (low-mass stars, with crustal neutron pairing and/or accreted low-Z envelopes) drop very rapidly below $T_\infty = 10^6$ K after 10^5 yr. Thus, if we interpret the thermal emission as full surface emission, it seems impossible for PSR J0538+2817 to be as old as its characteristic age. In contrast, its thermal surface emission is quite consistent with its young $\sim$30 kyr kinematic age, requiring no direct Urca process or any other exotic cooling mechanisms.

XMM-Newton observations find a low 18% soft X-ray pulsation with a very broad profile (McGowan et al. 2003). These authors interpret this as a hot polar cap from a nearly aligned rotator (polar cap axis and rotation axis both close to the line of sight). This seems at odds with the radio polarization and PWN data, so

a more natural interpretation might be emission from a gradual temperature variation across a light element surface, perhaps caused by magnetic dipole variation in the thermal conductivity (Greenstein & Hartke 1983).

If interpreted as a reheated cap emission the thermal flux would be a surprisingly large 1% of the full spin-down power. On the other hand, the nonthermal emission from the pulsar/PWN system as a whole is close to that expected. In an aperture of radius 15″, the observed count rate in the 2–10 keV band is 5×10^{-3} counts s^{-1}. After subtracting the background and thermal emission from the pulsar, the nonthermal contribution gives 2.8×10^{-3} counts s^{-1}. For a power law of $\Gamma = 1.5$, this converts to the luminosity of $10^{31.26}$ ergs s^{-1}. Possenti et al. (2002) found an empirical relation between the X-ray flux in the 2–10 keV band and spin-down luminosity: $\log L_{X,(2-10)} = 1.34 \log L_{sd} - 15.34$. For the case of PSR J0538+2817, the spin-down luminosity derived from the radio parameters (Anderson et al. 1996) is $L_{sd} = 5 \times 10^{34}$ ergs s^{-1}, which predicts an X-ray luminosity of $L_{X,(2-10)} = 10^{31.2}$ ergs s^{-1}, very close to the observed value.

6.7. *Conclusions*

We have reported VLBA astrometric measurements and *Chandra* ACIS-I observation of PSR J0538+2817. The VLBA astrometry gives the pulsar distance of $1.47^{+0.42}_{-0.27}$ kpc with a precise model-independent transverse velocity $V_{\perp} = 400^{+114}_{-73}$ km s^{-1}. These observations strengthen the association with S147 and suggest NGC 1960 as plausible birth site for the progenitor star. It seems likely that the supernova occurred in a stellar wind bubble some 40 kyr ago. The X-ray observations of the pulsar show that the thermal point source has a high temperature consistent with the 40 kyr age and imply that it was the source of the observed SNR. Our deep *Chandra* pointing reveals extended emission around the pulsar with a very compact symmetric structure observed in the 4–8 keV range. The overall PWN flux is broadly consistent with the emission expected from this relatively low $\dot{E}$ spin-down pulsar, but the physical origin of the hard emission in these innermost regions is not clear. Statistical arguments suggest that the symmetric emission is an equatorial structure, viewed edge-on, so that the pulsar spin and motion are roughly aligned, as for many other young pulsars. However, further observations are needed to reach definitive conclusions.

We thank Andrew Lyne for providing the current ephemeris of PSR J0538+2817. The initial VLBA observations of PSR J0538+2817 were made as part of the VLBA pulsar astrometry project (http://www.astro.cornell.edu/∼shami/psrvlb). The Hα image of S147 is based on data obtained as part of the INT Photometric Hα Survey of the northern Galactic plane: prepared by Albert Zijlstra, University of Manchester, and Jonathan Irwin, IoA Cambridge. The National Radio Astronomy Observatory is a facility of the National Science Foundation operated under cooperative agreement by Associated Universities, Inc. This work was supported by NASA grant NAG5-13344 and by *Chandra* grant G05-6058 issued by the Chandra X-Ray Center, which is operated by the Smithsonian Astrophysical Observatory for and on behalf of the National Aeronautics Space Administration under contract NAS8-03060.

Facilities: CXO(ACIS), VLBA

REFERENCES

Anderson, S. B., Cadwell, B. J., Jacoby, B. A., Wolszczan, A., Foster, R. S., & Kramer, M. 1996, ApJ, 468, L55
Cordes, J. M., & Lazio, T. J. W. 2002, preprint (astro-ph/0207156)
Davis, J. E. 2001, ApJ, 562, 575
Dehnen, W., & Binney, J. J. 1998, MNRAS, 298, 387
Dias, W. S., Alessi, B. S., Moitinho, A., & Lepine, J. R. D. 2002, A&A, 389, 871
Drew, J. E., et al. 2005, MNRAS, 362, 753
Faucher-Giguère, C.-A., & Kaspi, V. M. 2006, ApJ, 643, 332
Fich, M., Blitz, L., & Stark, A. 1989, ApJ, 342, 272
Greenstein, G., & Hartke, G. J. 1983, ApJ, 271, 283
Gvaramadze, V. V. 2006, A&A, 454, 239
Hobbs, G., Lorimer, D. R., Lyne, A. G., & Kramer, M. 2005, MNRAS, 360, 974
Johnston, S., Hobbs, G., Vigeland, S., Kramer, M., Weisberg, J. M., & Lyne, A. G. 2005, MNRAS, 364, 1397
Kharchenko, N. V., Piskunov, A. E., Roeser, S., Schilbach, E., & Scholz, R.-D. 2005, A&A, 438, 1163
Kirshner, R. P., & Arnold, C. N. 1979, ApJ, 229, 147
Kramer, M., Lyne, A. G., Hobbs, G., Löhmer, O., Carr, P., Jordan, C., & Wolszczan, A. 2003, ApJ, 593, L31
Kundu, M. R., Angerhofer, P. E., Fürst, E., & Hirth, W. 1980, A&A, 92, 225
Lozinskaya, T. A. 1976, Soviet Astron., 20, 19
McGowan, K. E., Kennea, J. A., Zane, S., Córdova, F. A., Cropper, M., Ho, C., Sasseen, T., & Vestrand, W. T. 2003, ApJ, 591, 380
Mel'nik, A. M., & Efremov, Y. N. 1995, Astron. Lett., 21, 10
Mori, K., Tsunemi, H., Miyata, E., Baluta, C. J., Burrows, D. N., Garmire, G. P., & Chartas, G. 2001, in ASP Conf. Ser. 251, New Century of X-Ray Astronomy, ed. H. Inoue & H. Kunieda (San Francisco: ASP), 576
Pavlov, G. G., Shibanov, Yu. A., & Zavlin, V. E. 1991, MNRAS, 253, 193
Phillips, A. P., Gondhalekar, P. M., & Blades, J. C. 1981, MNRAS, 195, 485
Possenti, A., Cerutti, R., Colpi, M., & Mereghetti, S. 2002, A&A, 387, 993
Romani, R. W. 2005, in ASP Conf. Ser. 328, Binary Radio Pulsars, ed. F. A. Rasio & I. H. Stairs (San Francisco: ASP), 337
Romani, R. W., & Ng, C.-Y. 2003, ApJ, 585, L41
Ruprecht, J., Balazs, B., & White, R. E. 1983, Soviet Astron., 27, 358
Sallmen, S., & Welsh, B. Y. 2004, A&A, 426, 555
Sofue, Y., Fürst, E., & Hirth, W. 1980, PASJ, 32, 1
Souvageot, J. L., Ballet, J., & Rothenflug, R. 1990, A&A, 227, 183
Sun, X., et al. 1996, in Rontgenstrahlung from the Universe, ed. H. U. Zimmerman et al. (MPE Rep. 263; Garching: MPE), 195
Sun, X. H., & Han, J. L. 2004, MNRAS, 350, 232
van der Swaluw, E. 2001, Ph.D. thesis, Universiteit Utrecht
Yakovlev, D. G., & Pethick, C. J. 2004, ARA&A, 42, 169
Yusifov, I., & Küçük, I. 2004, A&A, 422, 545
Zavlin, V. E., Pavlov, G. G., & Shibanov, Yu. A. 1996, A&A, 315, 141